PHYSICAL REVIEW B VOLUME 49, NUMBER 18 1 MAY 1994-II

Variation of interatomic distances in ice VIII to 10 GPa

J. M. Besson, Ph. Pruzan, and S. Klotz
Physique des Milieux Condensés, Université Pierre et Marie Curie, B 77, 4, place Jussieu, F-75252 Paris, France

G. Hamel
Département des Hautes Pressions, Université Pierre et Marie Curie, B 77, 4, place Jussieu, F-75252 Paris, France

B. Silvi
Laboratoire de Dynamique des Interactions Moléculaires, Université Pierre et Marie Curie, 4, place Jussieu, F-75252 Paris, France

R. J. Nelmes, J. S. Loveday, and R. M. Wilson
Department of Physics and Astronomy, The University of Edinburgh, Edinburgh EH9 3JZ, United Kingdom

S. Hull
ISIS Facility, Rutherford Appleton Laboratory, Chilton, Didcot, Oxfordshire OX11 0QX, United Kingdom
(Received 6 December 1993)

The pressure dependence of the structural parameters of deuterated ice VIII has been studied by time-of-flight neutron powder diffraction up to 10 GPa. Variations of the a and c parameters of tetragonal ice VIII, as well as those of the internal atomic coordinates of oxygen and deuterium are reported and discussed. Isothermal equations of state for ice VIII between 0 and 300 K are established. A periodic Hartree-Fock calculation performed at the all-electron level is shown to reproduce the equation of state at 0 K and the pressure dependence of the structural parameters, including the unexpectedly small variation of the O-D bond length up to 10 GPa. It also exactly accounts for the decrease under pressure of the A_{1g} vibron frequency in ice VIII, which is shown not to be caused by an increase of the covalently bonded O-D distance.

I. INTRODUCTION

The phase diagram of ices under high pressure has aroused lively interest for several decades. This is partly due to the fundamental character of the H_2O (D_2O) molecule in physical chemistry, and also to the fascinating variety of ice polymorphs which exist under different conditions of pressure and temperature. Above some 2 GPa, the phase diagram simplifies down to only two well-characterized solids: cubic ice VII with space group $Pn3m$ (O_h^4) and tetragonal ice VIII with space group $I4_1/amd$ (D_{4h}^{19}). The phase boundary between the two has recently been investigated by Raman scattering,[1,2] and its shape in the (p,T) plane accounted for, as a paraelectric-antiferroelectric phase transition line. Another result from these studies is to place the transition from ice VIII to the still hypothetical "symmetrized" ice X well above 50 GPa, in contrast with a number of previous expectations based on experimental indications[3,4] or theory.[5–8] In most cases, it had been assumed that the covalently bonded O-H distance regularly increased while the hydrogen bonded O-O distance did decrease under pressure,[9] in the same way as the O-H distance was known to increase with decreasing O-O distance in a variety of chemical compounds with O-H $\cdots$ O sites.[10] From this empirical relationship theoretical calculations[5,11] or fits of the measured decrease under pressure,[12,13] of the symmetric A_{1g} vibron frequency in D_2O or H_2O, both led to an expectation of an initial increase of the O-H (or O-D) distance by some 0.2–0.3 pm GPa^{-1}. Actually we have recently shown[14] that this behavior was not observed in neutron-scattering experiments on ice VIII under high pressure to 10 GPa. To the best of our knowledge these experiments are the first to date where the variation of the covalent bond length of a hydrogen (deuterium) atom has been measured over a sufficient pressure range to evaluate its pressure coefficient. Previous neutron-scattering experiments[15,16] in the 2.5-GPa range on ices VII and VIII had yielded their structural parameters at one pressure value only and therefore could not gauge the variation of the O-D distance with variable O-O separation continuously in the same crystal structure.

In this paper, we shall first describe fully the experimental conditions and procedure that were briefly mentioned[14] in our previous work. To analyze our data and compare them with theory, we shall then establish in Sec. III an equation of state for D_2O VIII versus temperature and pressure. Our results will then be analyzed and compared with an *ab initio* Hartree-Fock calculation, which is found to reproduce the observed pressure dependence of the lattice parameters a and c, and of the three internal coordinates. In addition, the effective potential for the deuteron which can be derived from this calculation is shown to account for the observed decrease of the A_{1g} vibron frequency under pressure.

0163-1829/94/49(18)/12540(11)/$06.00

II. EXPERIMENTAL PART

A. Instrumental details

The high-pressure anvils used here have a toroidal geometry[17] which has been devised mostly for high-pressure synthesis and has been adapted to time-of-flight neutron-scattering measurements.[18,19] Figure 1 shows the experimental volume which contains the sample (1) to be pressurized. Its diameter is 6 mm and its thickness along the axis is about 4 mm, which gives a volume of 85 $mm.^3$ The flat washer and toroidal gasket (2) may be made of various metals or alloys. A null-scattering TiZr alloy was found to be the best choice, since it avoids Bragg edges, and has sufficient mechanical strength to reach ~10 GPa in this single toroid arrangement. The anvils (3) are K 10 tungsten carbide dies, 18 mm in diameter, from Sandvik Hard Materials. They rest on seats (4) made of the same alloy, 40 mm in diameter. Both the anvils and the seats have a 1.5° angle on the outer surface, and are shrunk at ambient temperature into steel binding rings (5), which exert a radial supporting stress of 1 to 1.2 GPa. The seats are drilled with ϕ 5-mm bore (6) for the incident neutron beam (i) and a recess at the back of the anvils (7) leaves a thickness t of tungsten carbide for the incident neutrons to traverse. It was found that $t=5$ mm was sufficient to reach pressures above 10 GPa with no systematic failure. At this pressure, the 5-mm-thick WC dome sustains a load of at least 25 metric tonnes.

Diffracted neutrons are detected over a range of 14° centered at $2\theta=90°$ and the emergent beam (e) which is transmitted through the anvils and sample space, can also be measured on a back detector, to calibrate the corrections for absorption and Bragg edges in the anvil material. An absorbing layer covers the anvil faces and sides (a). This can be Gd_2O_3 paint, or, preferably a 0.1-mm electroplated layer of cadmium. With this setup, most of the detected neutrons (d_1) only traverse the null-scattering gasket material. Nevertheless, a sizeable number (d_2) have to go through the tungsten carbide of the anvils.

In order to compress such an arrangement to ~10 GPa, a force of 110–135 tonnes (~ 1.1–to 1.35 MN) is required. For our neutron-scattering measurements, we had to build hydraulic presses which would fit into the ϕ 400-mm tank of the POLARIS station of the ISIS spallation source at Rutherford Appleton Laboratory. Their capacity is 250 tonnes and their mass only ~50 kg. The principle of their construction has been described before.[20–22] In the work described in Refs. 20–22 a simple ram was used. In order to monitor the transmitted neutron beam ("e" in Fig. 1) we found it advantageous to use a hollow ram[23] such as shown in Fig. 2. The press with the sample and anvils is used with its axis in a horizontal position at the POLARIS station. The diffracted signal is recorded by a set of ZnS detectors designed and built for

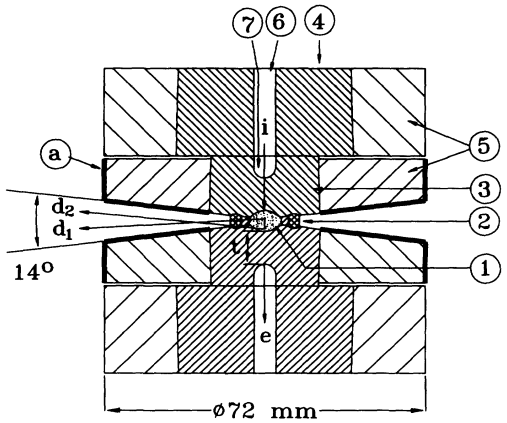

FIG. 1. High-pressure assembly. (1) Sample space is 6 mm in diameter. (2) Gasket assembly (Ti:Zr null scattering alloy) ~15 mm initial diameter. (3) Tungsten carbide anvils K10 Sandvik Hard Materials). (4) Tungsten carbide seats: same material. (5) Binding rings: 35 NCD 16 alloy steel (819 AW Aubert et Duval) 72 mm in outside diameter. The frettage gives 1.0 GPa radial compressive support to the anvils and seats. (6) 5-mm bore which collimates the incident neutron beam (i). (7) Recess in the anvils diminishes the absorption of the incident neutron beam. Spherical shape at the bottom is for mechanical strength. The remaining WC between the bottom of the recess and that of the sample cup has a thickness (t) which may range from 5 to 7 mm. (e) Outgoing beam used for calibration measurements. (a) Absorbing material (Gd_2O_3 or Cd) which defines a 14° viewing angle to the detector banks. (d) Diffracted neutrons path. d_1 goes through the TiZr gaskets only. d_2 also goes through the anvils and has, in addition, to be corrected for the Bragg edges of the anvils material.

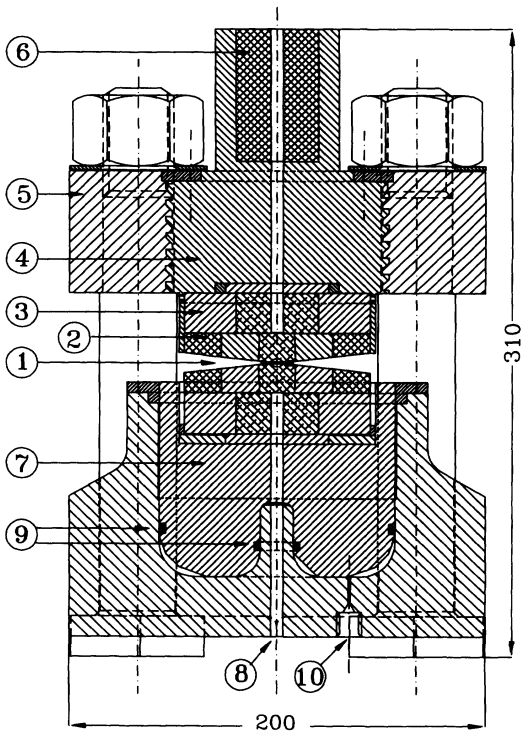

FIG. 2. Cross section of the V4 Paris-Edinburgh press. (1) Sample and gaskets. Sample is ϕ6 mm. (2) Anvils and supporting rings. (3) Seat assemblies. (4) Breech. (5) Platen. (6) Boron carbide collimator with ϕ5-mm hole for the incident beam. (7) Piston with ϕ5-mm central hole. (8) Outgoing neutron beam path. (9) Inner and outer sealing "O" rings. (10) Low-pressure hydraulic fluid inlet. Dimensions are in millimeters.

this application.[23] They cover an angular range of ±7 degrees about the 90° scattering direction and a total of 130° around the beam axis. Their effective resolution is $\Delta d/d = 6\times10^{-3}$.

B. Experimental procedure

The samples used are 99.8% enriched D_2O obtained from EURISO-TOP (CEA). D_2O is used rather than H_2O to avoid the high background of incoherent scattering from the H atom in the neutron-diffraction spectra. The loading is done at room temperature[18,21] and the sample pressurized also at ambient temperature. Cooling to 265 K is achieved by flowing cold N_2 gas on the anvils and gasket. The press rests inside an aluminum vessel, under a dry nitrogen atmosphere, to prevent condensation of ice on the anvils. Temperature is measured by a thermocouple on the gasket, so that the sample's actual temperature may have been 2–4° above 265 K. All the data points presented here have been obtained by pressurizing the sample to the required pressure at ambient temperature in ice VII, and then cooling while the ram's oil pressure was kept constant, i.e., the sample and cell were warmed up to 280 K to ice VII prior to any pressure increase, and then quasi-isobarically cooled. This procedure is time consuming but was found to give reproducible results, as regards crystal parameters, notably c/a, which is quite sensitive to nonhydrostatic stresses in the sample. By contrast, spectra taken when the pressure was increased at low temperature (265 K), in ice VIII, show from loading to loading variations up to 5×10^{-3} in the c/a ratio. The removal of this effect, by pressurizing the sample at 280 K, may tentatively be assigned to the relieving of non-hydrostatic stresses in the sample during the VII→VIII transition, small as the volume change ($\Delta V/V \leq 10^{-3}$) may be.[15,24] Spectra were collected at eight applied loads between 0.65 and 1.35 MN, always on the upstroke, since decreasing the pressure in a controlled way in toroidal anvils with metal gaskets, was found to be difficult. Decreasing the load consistently leads to a rapid decompression of the sample which, on occasion, causes failure and ignition of the gasket, since zirconium is pyrophoric in air, under shock.

Collection of data was done for 4–8 h amounting to some 600–800 μA h of proton current on the POLARIS station. Spectra were corrected for the attenuation of the in- and out-going beams as described before.[14,19] An additional correction was applied to account for the displacement of the sample along the cell's axis, under the thrust of the ram. This displacement is directly measured and amounts to over 2 mm at the highest pressure, which corresponds to a correction of $\sim10^{-3}$ on the lattice parameters. The corrected spectra were analyzed by the Rietveld refinement procedures using the GSAS refinement package.[25] In the $I4_1/amd$ tetragonal space group of ice VIII, the oxygen atoms are at [0,1/4, z(O)] and the deuterium atoms at [0,y(D), z(D)], which, with the a and c parameters, makes up five independent structural parameters. In addition we have varied two isotropic thermal parameters, a background polynomial, four peak-width parameters, and the sample absorption. The quality of the resulting fits is shown in Fig. 3. In this figure, the circle and arrow show the only sign of stray signal from the tungsten carbide anvils which collimation did not eliminate. The intensity of this unwanted signal must be compared to the mass (1 Kg) of the anvils which surround the sample (0.1 g). This well demonstrates the capabilities of time-of-flight measurements where careful collimation of the in- and out-going beams can virtually eliminate all pollution from the sample's environment. In order to obtain the cleanest possible patterns, no calibrant was used for these measurements and the pressure was derived from the equation of state (a and c parameters) of ice VIII. Since this has not been measured, it had to be calculated as described in the next section.

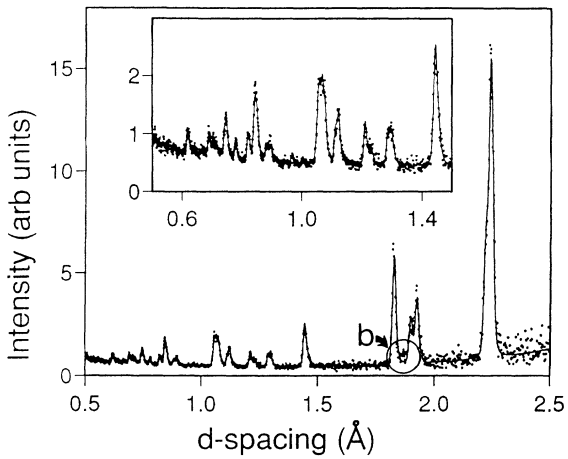

FIG. 3. A spectrum collected from a sample of ice VIII at 9.9 GPa. The dots are measured data. Solid line is the result of a one-phase Rietveld profile refinement. "b" is the only detectable Bragg peak from the background from the tungsten carbide anvils (circle).

III. EQUATION OF STATE OF ICE VIII

The equation of state (EOS) of ice VIII at 265 K must be known in order to determine the pressure of the samples in our measurements. The EOS at zero K is also needed to allow comparison with theory (Secs. V and VI). In this section, we will evaluate the $V(p)$ dependence of ice VIII between 0 and 300 K, using available experimental data, and the universal equation of state[26,27] proposed by Vinet *et al.* In the present calculation, we shall not distinguish between regions in the p-T plane where ice VIII is totally stable ($T<278$ K; $p>2.2$ GPa) and regions where it is only metastable ($p=0$ GPa; $T<135$ K) or completely unstable (e.g, $T=300$ K). The EOS of ice VIII will be calculated for all the pressure temperature domain: $0<p<12$ GPa and $0<T<300$ K.

A. Equation of state at 300 K

The volume of ice VIII is taken to be the same as that of ice VII since the volume difference ΔV between the two is immeasurably small[15,24] with $\Delta V/V \leq 10^{-3}$. This behavior is related to the very steep slope of the VIII-VII phase transition line in the p-T plane. It has been shown to remain so[1,2] well above 10 GPa, so that presumably $\Delta V/V$ also remains small up to the maximum pressure of

our experiments. For the equation of state of ice VII (or VIII) at 300 K we used the published data[28] of Hemley *et al.* which are the latest measurements on the subject and rest on the most reliable pressure scale to date. In the low-pressure region, these data do not entirely coincide with previously published measurements,[12,29,30] but the agreement is sufficient for our purpose. The equation of state of D_2O and H_2O were taken to be identical within experimental accuracy, as shown[29] on D_2O and H_2O VII. In using the results of Ref. 28, we do not retain the values of B_0 (bulk modulus), B' (its derivative: $[dB/dp]_{p=0}$), and V_0 calculated in this reference, which are for a best fit up to 100 GPa and include data with good precision (below 18 GPa) and data with poorer precision, above 18 GPa. Since our purpose is to get the best possible EOS up to 10 GPa, we fitted the data given in the table of Ref. 28 up to 18 GPa with a Birch-Murnagham equation of state:

$$p=3/2B_0[(V_0/V)^{7/3}-(V_0/V)^{5/3}] \times\{1+3/4(B'-4)[(V_0/V)^{2/3}-1]\} . \quad (1)$$

The best fit is with

$$V_0=12.45 \text{ cm}^3/\text{mol} , \quad B_0=20.4 \text{ GPa} , \quad B'=4.7 ,$$

which is a little different from the values of Ref. 28:

$$V_0=12.30 \text{ cm}^3/\text{mol} , \quad B_0=23.7 \text{ GPa} , \quad B'=4.15 .$$

B. Temperature dependence of the volume at $p=0$

The next step is now to evaluate the thermal expansion of D_2O VIII, or preferably the temperature dependence of the volume at zero pressure of ice VIII. No low-temperature data exist except work by Kamb and Prakash[31] quoted by various authors which gives a volume of 12.12 ± 0.07 cm^3/mol at 108 K. In addition, for the present calculation, we could use direct measurements, made at the HRPD station of the ISIS spallation source by Ross, Li, and Bokhenkov, of the diffraction patterns of a metastable ice VIII sample between 78 and 135 K. This sample which has been made under high pressure and depressurized at 77 K has given diffraction patterns showing five diffraction peaks, (112), (200), (103), (211), and (202) up to 130 K. From these data the lattice parameters and molar volume could be obtained (Fig. 4). Although the temperature was not stable, the precision of the measurements is sufficient for our purpose. Using the data at 300 K and at low temperature, a best-fit curve for the variation of the molar volume with temperature $V(T)$ can be drawn using the formulation of Vinet *et al.* [Eq. (5.1) of Ref. 27] which reads

$$3/X^2(1-X)\exp[3/2(B'-1)(1-X)]+\alpha(T-300)=0 \quad (2)$$

with $X=(V/V_0)^{1/3}$; the molar volume at 300 K is $V_0=12.45$ cm^3/mol; $B'=4.7$ at 300 K as determined from Eq. (1); α, the cubic thermal expansion coefficient at 300 K is determined by the best fit of Eq. (2) with the experimental data. It is

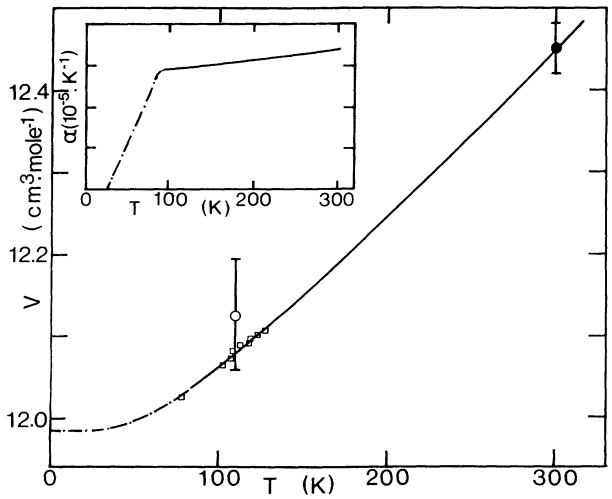

FIG. 4. Molar volume of D_2O VIII as temperature, at ambient pressure. Full circle: Volume at 300 K (Table I). Hollow circle: Volume at 108 K (Ref. 31). Hollow squares: Volume between 80 and 125 K (see text). Full line: Best fit of data with Eq. (2). Dash dotted line: Integration of dash dotted line of the insert. Full line: Volume expansion coefficient obtained by derivation of the full line of the figure. Dash-dotted line approximates the expected variation of $\alpha(T)$ between ~100 and 0 K.

$$\alpha(300 \text{ K})=1/V[\delta V/\delta T]_p=17\times10^{-5} \text{ K}^{-1} . \quad (3)$$

This value compares with the thermal expansion of ice I_h at 300 K which is[32] 16×10^{-5} K^{-1} and that of ice VI at ~1 GPa which is[33] 16×10^{-5} K^{-1}. Equation (2) is not valid at very low temperatures and it has been shown to be accurate[27] only above 100 K for NaCl, above 200 K for gold, and above 40 K for xenon, for instance. In the present case, it must not be valid below ~100 K. At low temperature we take a form for the thermal-expansion coefficient which is shown in the inset of Fig. 4 as a dash-dotted line, the integration of which gives the dash-dotted part of the $V(T)$ curve. This is similar to the general behavior of $\alpha(T)$ at low temperature for those solids where it has been measured.[34] This procedure is only approximate but the actual shape of the decrease of α from its 100 K value to zero has very little influence on the absolute value of V (0 K), which will vary by less than 1% whatever the temperature dependence of $\alpha(T)$ is taken to be below 100 K.

C. Equation of state $V(p)$ at variable temperature

With these value of $V_0(T)$ and $\alpha(T)$ at ambient pressure, we are now in a position to derive the equation of state of D_2O VIII at any temperature between 0 and 300 K, by calculating the parameters $B_0(T)$ and $B'(T)$ of a Birch-Murnaghan equation of state. These are given by Eqs. (4.5) and (4.6) of Ref. 27. In the present case, they read

$$B_0(T)=B_0/X^2[2+(\eta-1)X-\eta X^2]\exp[\eta(1-X)] , \quad (4)$$

$$B'(T)=\frac{4+(3\eta-1)X+\eta(\eta-1)X^2-\eta^2X^3}{3[2+(\eta-1)X-\eta X^2]} \quad (5)$$

with $\eta=3/2[B'-1]$, $X=[V_0(T)/V_0(300\text{ K})]^{1/3}$ $V_0(T)$ is the molar volume at temperature T, $V_0(300\text{ K})$ is the molar volume at 300 K: 12.45cm^3/mol, B_0 is the bulk modulus at 300 K: 20.4 GPa, B' is its derivative $[dB/dp]_{p=0}$ at 300 K: 4.7 We thus can calculate the temperature dependence of B_0 and B' which, together with V_0, will be used to derive the $V(p)$ isothermal equations of state. Table I gives the parameters found from Eq. (4) and (5) and Fig. 4.

Curves for $V(p)$ at different temperatures are given in Fig. 5, calculated from Eq. (1) and the parameters of the table. In this procedure, there is an apparent inconsistency which is the use of the Vinet equation of state to calculate the temperature effects, while applying them to the parameters of a Birch-Murnaghan equation of state, and not of a Vinet EOS which has a different mathematical form. This was done for convenience: The Birch-Murnaghan form is that which is most commonly used in the literature. In the present case, we use the Vinet EOS to correct room-temperature values of B_0 and B' by a small fraction only and the relative change in those parameters when going from 300 to 0 K is the same whether one takes the B_0 and B' from Vinet's EOS or from a Birch-Murnaghan EOS. The validity of the EOS shown in Fig. 5 is entirely dependent on the data selected at the start[28] that is Hemley's EOS for H_2O VII at 300 K. This choice, has been justified above, but if "better" data are published in the future, the $V(p,T)$ dependence can be redetermined in a straightforward fashion along the lines used here. Comparison with experiment is shown in Fig. 5 with the data of Ref. 31 at 108 K and one 10 K value from Ref. 15: $V=11.06$ cm^3/mol at 2.4 GPa. A problem exists for the 265 K isotherm: Two values are given in the literature, around 265 K: from neutron-scattering measurements. These are

$V=11.18$ cm^3/mol at 2.4 GPa (Ref. 15),

$V=11.21$ cm^3/mol at 2.8 GPa (Ref. 16).

This is clearly inconsistent since the volume can only decrease under pressure, so that these points cannot be used for a fit of our $V(p)$ curve. In any case, our 265-K isotherm happens to be (Fig. 5) in between those two values: $V=11.20$ cm^3/mol at 2.66 GPa. Although Fig. 5 and Table I provide EOS parameters which fit well with available experimental data, they do not allow extrapolation

TABLE I. Equation-of-state parameters for D_2O VIII for a Birch-Murnaghan equation to third order [Eq. (1)]. Those are *ad hoc* parameters, which are meant to represent the $V(p)$ behavior of D_2O VIII in the range of our experiments (0–10 GPa). They should not be used for higher pressures (see text).

Temperature K	V_0: cm^3/mol	B_0: GPa	B'
300	12.45	20.4	4.70
265	12.38	21.0	4.66
100	12.06	23.6	4.48
0	11.98	24.1	4.44

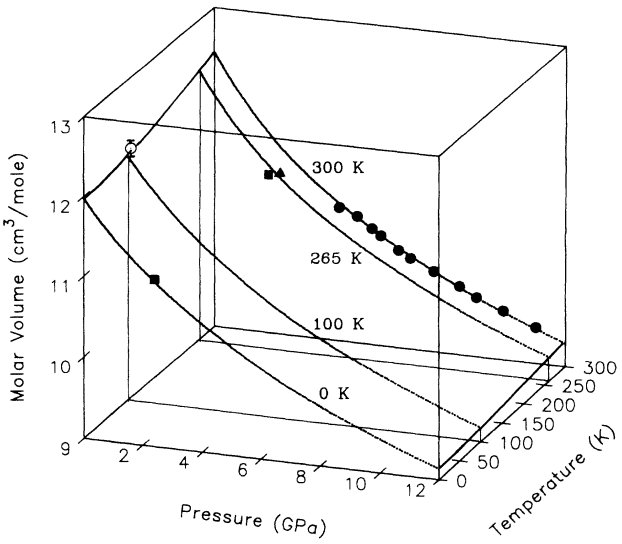

FIG. 5. Molar volume of ice VIII *versus* temperature and pressure. Lines are drawn for the four temperatures of Table I with a Birch-Murnaghan equation to third order [Eq. (1)]. Full circles: Experimental data at 300 K from Ref. 28. Full squares: Experimental data at 263 and 10 K from Ref. 15, at 24 GPa, Full triangle: Experimental point at 265 K and 28 GPa from Ref. 16. Hollow circle: Experimental point at ambient pressure and 108 K from Ref. 31.

outside the pressure and temperature range for which this calculation was done: This is, 300 K and ~10 GPa. In particular, to extend this EOS to higher pressures, e.g., 100 GPa, the best-fit parameters of Ref. 28 should be utilized, and the calculation performed again with this new set.

IV. EXPERIMENTAL RESULTS

The results of the refinements of the spectra, and the corresponding pressures calculated from the 265-K isotherm are given in Table II. The pressures are slightly different (by 0.1 GPa or so) from those listed in our previous paper[14] where the thermal correction procedures had not been made in the same manner. This has no bearing on the interpretation of the results.

The main result as noted before[14] is the very small variation of the covalently bonded O-D distance r with pressure. The very small magnitude obtained from this is quite different from that which was previously assumed, on the basis of its variation in a number of chemical species at ambient pressure, as a function of $R(O\cdots O)$, the distance between hydrogen-bonded oxygen sites. The increase of r(O-D) [or r (O-H), which is expected to be identical] versus pressure had been predicted to assume different values, depending on the compounds that were examined. The values that have been put forward are 0.18 pm GPa^{-1} in Ref. 13, 0.25 pm GPa^{-1} in Refs. 11 and 5, and as high as 0.35 pm GPa^{-1} in Ref. 12.

The observed variation is 0.04±0.04 pm GPa^{-1}: that is, significantly smaller. In the lower pressure range (2.7 GPa) our values for the internal atomic coordinates and

TABLE II Structural parameters of D_2O VIII versus pressure. Values of the pressure are slightly different from those given in Ref. 14, p. 1194, for reasons given in the text. Accuracy on V and p depends on the 300 K equation of state which is chosen and thus, no error can be quoted on those quantities. Figures in parentheses are the estimated standard deviations from the refinements.

Load MN	a nm	c nm	c/a	V cm^3/mol	p GPa	r(O-D) pm	z(O)	y(D)	z(D)
0.65	0.467 44 (4)	0.679 72 (9)	1.4541 (4)	11.182	2.7	97.23 (30)	0.1080 (4)	0.4170 (6)	0.1937 (4)
0.72	0.464 41 (3)	0.674 4 (1)	1.4522 (4)	10.951	3.4	97.18 (26)	0.1098 (4)	0.4190 (5)	0.1951 (4)
0.83	0.459 15 (3)	0.665 68 (9)	1.4498 (4)	10.566	4.8	97.33 (27)	0.1104 (4)	0.4205 (6)	0.1976 (4)
0.94	0.455 00 (4)	0.658 02 (10)	1.4462 (4)	10.256	6.1	97.67 (27)	0.1102 (4)	0.4228 (6)	0.1986 (4)
1.05	0.451 65 (4)	0.652 3 (1)	1.4443 (4)	10.018	7.3	97.37 (26)	0.1103 (4)	0.4231 (6)	0.1997 (4)
1.15	0.449 09 (4)	0.648 4 (1)	1.4438 (4)	9.845	8.2	97.58 (25)	0.1096 (4)	0.4242 (6)	0.2000 (4)
1.25	0.446 55 (3)	0.644 2 (1)	1.4426 (4)	9.671	9.3	98.02 (24)	0.1101 (4)	0.4264 (6)	0.2011 (4)
1.35	0.444 93 (4)	0.641 3 (1)	1.4414 (4)	9.558	9.9	97.12 (28)	0.1106 (4)	0.4256 (6)	0.2011 (5)

for the O-D distance fit, within experimental accuracy, with previously published neutron-scattering data.[15,16] The values for θ, the D-O-D angle are not included in the table since they do not vary within an estimated standard deviation (e.s.d) of half a degree, and actually were constrained to 106.5 degrees without any alteration of the fit.[14] The uncertainties given in parentheses in the table are the e.s.d.'s obtained in the refinements. As noted in Sec. II, other experiments were performed with the pressure being increased at low temperature. The results are of lower quality, as shown by the irregular behavior of c/a vs p. Nevertheless, in each series of runs, the refinements consistently yield a negligible variation of the O-D distance in accordance with the present results, although the average apparent absolute value of r(O-D) may differ by a fraction of a pm from that shown in Table II. This is to be assigned to the presence, in the sample, of preferred orientation and nonhydrostatic strains which are maintained under increasing pressure. This causes systematic intensity variations in individual diffraction peaks which in turn cause a systematic offset in the refined atomic coordinates.

In order to check on the consistency of these results a calculation was performed and compared with the experimental data.

V. METHOD OF CALCULATION

The calculations have been performed at the periodic Hartree-Fock level with the pseudopotential version of the CRYSTAL92 program developed in Torino.[35] A documented description of the method has been published by Pisani, Dovesi, and Roetti.[36] This method works within a single determinant approximation of the wave function in which the crystalline orbitals are expressed as a linear combination of Bloch functions which are themselves expressed in terms of the atomic basis functions of each unit cell. As input, the program requires geometry and basis set information together with a set of thresholds which controls the truncation of infinite sums. As output it provides the unit-cell energy, the wave function, and related one-electron properties.

The present calculation has been performed at the all-electron level with the standard 6–31 G** basis set,[37] the asterisks indicate that sets of d and p functions on oxygen and hydrogen centers, respectively, have been added to the standard sp and s shells. Extensive calculations on the water dimer[38] have shown that this basis set yields an optimized structure in qualitative agreement with those calculated with better basis sets involving diffuse s and p functions at the MP/2 level. At the present state of the art it is not possible to include diffuse basis functions in periodic calculations because they should produce basis set linear dependence. Diffuse functions are needed in molecular calculations in order to account correctly for the long-range exponential decay of the electron density whereas in crystals this problem is removed by the periodicity and therefore such functions are much less necessary. The agreement between 6–31 G** self-consistent field (SCF) and 6–311++G (2d,2p) MP/2 results is due to spurious error compensations. With respect to the Hartree-Fock limit, the monomer dipole moment is calculated 0.25 D too large by the 6–31 G** basis set. Therefore the intermolecular separation is found shorter by 3.8 pm and the electrostatic contribution to the interaction energy is overestimated by 1.4 kJ mol^{-1}. At short and intermediate intermolecular distances, this extra electrostatic energy partly compensates the missing dispersion energy. At larger distances, this yields an overcompensation because the dipole interaction decays as R^{-3} instead of R^{-6} for dispersion.

The neglect of electron correlation in Hartree-Fock calculations is the main weakness of this approximation with respect to density-functional theory (DFT) derived methods. The effect of this neglect can be dramatic for molecular crystals in which most of the cohesive energy is due to dispersion forces. In molecular calculations, the dispersion is introduced by perturbation, configuration interaction or coupled cluster techniques. In periodic systems, it is not possible to define excited configurations and therefore the previously mentioned techniques cannot be used to calculate the electron-correlation energy. However, local approaches such as the local-ansatz[39] or DFT method can be used to evaluate the local correlation (i.e., the Coulomb-hole contribution) in a post SCF step. In principle, these local approaches do not account for nonlocal correlation and therefore for the dispersion energy. Surprisingly, density functionals work quite well to evaluate dispersion energy at short and intermediate intermolecular distances. This is shown by the success of the Gordon-Kim[40] method for rare-gas solids[41] and atom-

ic dispersion coefficient evaluation[42] and also by recent results on brucite[43] in which it was demonstrated that the stacking of the layers is mostly due to van der Waals interaction. A possible way to account for dispersion is to correct the interaction energy with semiempirical atomic or molecular dispersion coefficients.

The reciprocal-space integration is performed using a commensurate net, the meshes of which are determined by the shrinking factor S. A value of $S=4$, corresponding to 24 k points, has been used for the present calculations. When $S=8$ is used the energy change is less than the SCF convergence threshold: 10^{-6}.

VI. RESULTS AND COMPARISON WITH EXPERIMENT

A. Structure optimization

The structure optimization has been automatically carried out with overhead conjugate gradient routines to the CRYSTAL92 program by D'Arco.[44] In this facility, the coordinates can be either standard crystallographic variables (i.e., lattice parameters and atomic fractional coordinates), internal coordinates (bond lengths, bond angles) or a mixing of both. The convergence of the optimization procedure is faster when the hessian matrix is almost diagonal. Internal coordinates yield force fields in which the diagonal constants are large and interaction (off-diagonal) constants are weak, and therefore are more suitable when they are easily available. Ice VIII belongs to the $I4_1/amd$ space group with oxygen and hydrogen, respectively, in 8e and 16h positions and is therefore described as noted above by two lattice parameters a and c and three atomic coordinates z(O), y(D), and z(D). This structure is made up of two intermingling hydrogen bonded networks of water molecules the relative positions of which are determined by the oxygen coordinate z(O). Instead of the five crystallographic variables, three internal coordinates—namely the water molecule bond angle θ, the O-H intramolecular bond length r and the O-O separation R, and the oxygen coordinate z(O) have been optimized. Experimentally[15] the hydrogen bond in ice VIII is almost linear. Moreover, the O-H-O bending being a very soft coordinate, the numerical differentiation procedure used in this conjugate gradient subroutine is not accurate enough to provide reliable results (i.e., emerging from the numerical noise). The hydrogen bond has therefore been constrained to be linear during the optimization process. With this assumption, the lattice constants and hydrogen fractional coordinates are given by

$$a=2R\sin(\theta/2)\,, \tag{6}$$

$$c=4R\cos(\theta/2)\,, \tag{7}$$

$$y(\mathrm{D})=\tfrac{1}{4}+\tfrac{1}{2}r/R\,, \tag{8}$$

$$z(\mathrm{D})=z(\mathrm{O})+\tfrac{1}{4}r/R\,. \tag{9}$$

In order to investigate the pressure dependence of ice VIII, structure optimizations have been also carried out for seven fixed O-O distances shorter than the equilibrium values allowing the calculation of the third-order Birch-Murnaghan equation-of-state parameters [Eq. (1)]. The calculated bulk modulus is $B_0=23.5$ GPa and its pressure derivative $B'=3.7$. Figure 6 displays the calculated and experimental variation of the calculated molar volume, compared with the experimental[28] 300 K values for ice VII and the 0 K values calculated in Sec. III. The agreement is satisfactory. The results of the geometry optimization at different R are reported in Table III along with the pressure estimated from the calculated equation of state.

At ambient pressure the c parameter is found to be too large by 20 pm. This rather large error is due to a small uncertainty on the intramolecular bond angle θ and to a slight overestimate of the O-O distance which is explained by the lack of dispersion energy in our calculation. An error of 10 pm on c is explained by an uncertainty of 1.2° in θ. The equilibrium geometry can be improved by taking the dispersion energy into account by means of semiempirical C_6 coefficients. Atomic coefficients[42] yield a dramatic decrease of the intermolecular distance to 2.77 Å, whereas molecular coefficients such as those proposed by Amos and Yoffe[45] or by Margoliash and Meath[46] provide more realistic results, i.e., $R=0.296$ and 0.293 nm, respectively.

For the equilibrium structure, the calculated cohesive energy of the crystal is -49 kJ mol^{-1}. With the Boys-Bernardi counterpoise correction[47] of the basis set superposition error, it is -36.4 kJ mol^{-1}. The missing contribution of dispersion energy evaluated with the C_6 value of Amos and Yoffe is -17.8 kJ mol^{-1} whereas the Margoliash and Meath value yields -22.18 kJ mol^{-1} both bringing the calculated value close to the experimental one.[48]

Figure 7 shows the c/a parameter *versus* molar volume, compared to our experimental results. Although the absolute value is too large by 1%, the variation of c/a *versus* molar volume is in complete agreement with experiment. The experimental variation of the c/a ratio follows a linear dependence with density. At this point one may speculate on the stability domain of tetragonal ice VIII under pressure. It is known[2] that this structure exists in a closed domain of pressure and temperature. At pressures below ~15 GPa the transition of ice VIII to

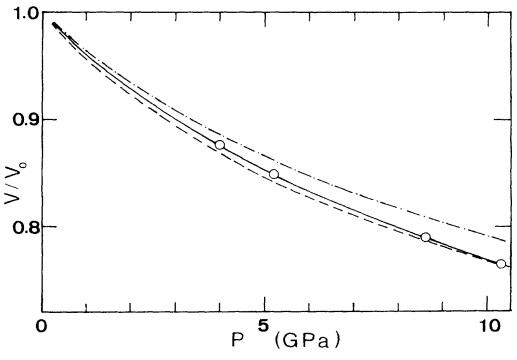

FIG. 6. Volume variation of ice VIII under pressure. Hollow circles and full line: Calculation (Table III). Upper curve, Dash-dotted line: Equation of state at zero temperature (Table I). Lower curve, Dashed line: Experimental equation of state at 300 K (Table I and Ref. 28).

TABLE III. Results of the Hartree-Fock calculation. The bottom three data sets are outside the range of our experiments and are not used for comparison. θ is the intramolecular bond angle.

p GPa	R nm	θ degrees	a nm	c nm	c/a	V cm^3/mol	r(O-D) pm	z(O)	y(D)	z(D)
0.0	0.303	106.9	0.4868	0.7218	1.4827	12.877	95.05	0.1122	0.4068	0.1906
4.0	0.290	107.3	0.4671	0.6876	1.4721	11.295	95.05	0.1125	0.4139	0.1944
5.2	0.287	107.4	0.4626	0.6796	1.4691	10.949	95.06	0.1125	0.4156	0.1953
8.6	0.280	107.6	0.4519	0.6615	1.4638	10.170	95.09	0.1125	0.4198	0.1974
10.3	0.277	107.6	0.4471	0.6534	1.4614	9.834	95.10	0.1125	0.4217	0.1983
15.1	0.270	108.2	0.4374	0.6333	1.4479	9.122	95.13	0.1125	0.4262	0.2006
24.2	0.260	108.2	0.4212	0.6098	1.4478	8.145	95.27	0.1131	0.4332	0.2047
36.9	0.250	108.3	0.4053	0.5857	1.4451	7.162	95.75	0.1162	0.4415	0.2120

cubic ice VII is purely due to thermal effects: The transition line is vertical in the (p,T) plane ($dT/dp=0$) and the volume variation negligibly small. On the contrary, at temperatures close to zero, $dp/dT=0$ and the transition to ice VII is due to pressure (density) only. Now, although we have data for c/a versus p at 265 K only, we can note that the only low-temperature value[15] at 10 K, is within 10^{-3} of the 265 K straight line (black square in Fig. 7). It is thus legitimate to expect the c/a ratio to have the same density dependence at low temperature. Now, if the transition from tetragonal ice VIII to cubic ice VII were gradual, one would expect, among other symptoms, the c/a ratio to go to $\sqrt{2}$ at the phase line. Extrapolation of our data to $c/a=\sqrt{2}$ gives a molar density of ~ 6 cm^3/mol, which corresponds[28] to a pressure of 70–75 GPa. This compares very well with the actual value of the transition for VIII to VII: 72 GPa at 0 K. This would support the hypothesis which has been put forward[2] that the first-order character of the VIII→VII transition vanishes at low temperatures.

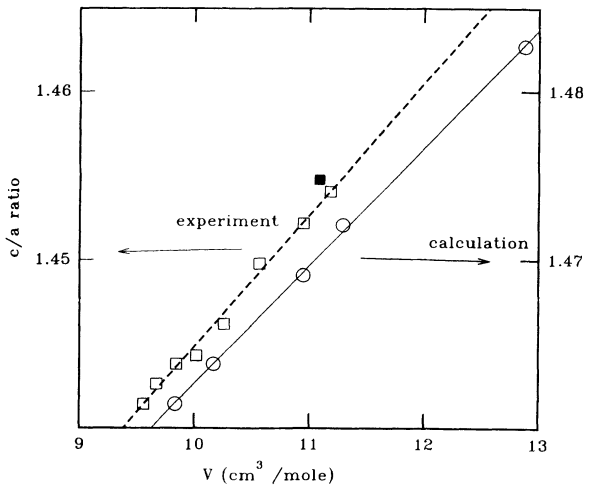

FIG. 7. c/a ratio *versus* molar volume. Empty squares and dashed line: Experiment (Table II): 265 K (left-hand ordinate scale). Full square: Experimental point at 10 K from Ref. 15. Empty circles and full line: Calculation (Table III): 0 K (right-hand scale). The right-hand ordinates have been shifted down by 0.02 with respect to the left-hand side, to allow comparison of the calculated and experimental variation of c/a vs molar volume.

Figures 8(a)–8(c) show the comparison of measured and calculated values for the three atomic coordinates z(O), y(D), and z(D) *versus* pressure. Although again, the absolute values are off by 1 or 2%, the pressure variation of the atomic fractional coordinates is quite well reproduced. In the lower pressure range, z(O) and z(D) exhibit

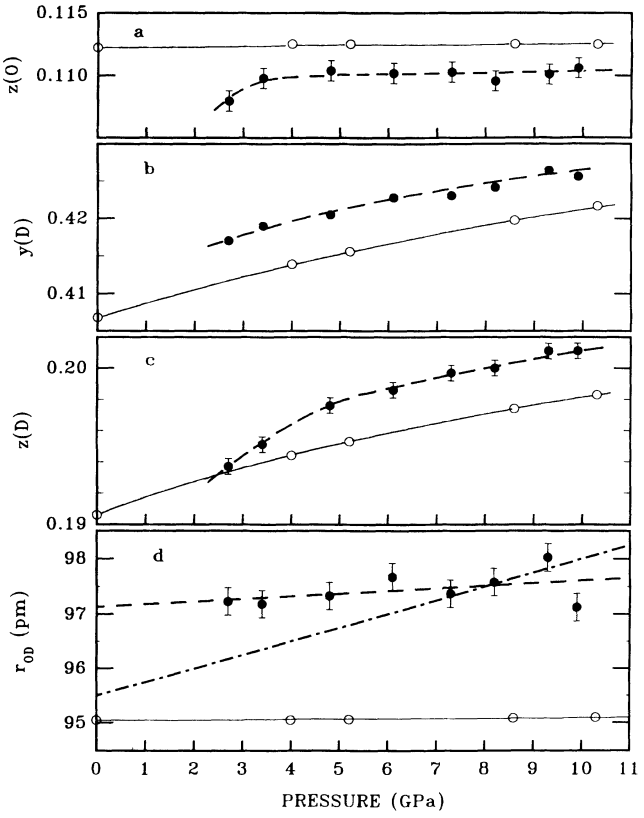

FIG. 8 Variation of the atomic coordinates under pressure. Full circles and dashed lines: Experiment (Table II). Empty circles and full lines: Calculation (Table III). Dashed and full lines are guides to the eye for (a), (b), and (c). (a) z(O): The internal atomic coordinate of the oxygen atom in the ice VIII tetragonal network would be 0.125 in a cubic structure. (b) y(D): The e.s.d's for this coordinate are smaller than the data points (Table II). (c) z(D). (d) Oxygen-deuterium intramolecular distance r. The dash-dotted line has a slope of 0.25 pm GPa^{-1} as predicted from Refs. 5 and 11–13. The dashed line has a slope of 0.04 pm GPa^{-1}.

a downward curvature which may be associated[14] with the transition to ice VI at 2.1 GPa.

Figure 8(d) shows the measured and calculated O-D distance *versus* pressure. The predicted change up to 10 GPa is immeasurably small, which essentially fits with our best estimate for the rate of change, that is 0.04 ± 0.04 pm GPa^{-1}. In any case the observed change is much smaller than the value (0.2–0.3 pm GPa^{-1}), which was expected from the behavior of the vibron frequency under pressure, and the calculation of the r vs R distance using a Morse double-well potential.

The behavior of z(O) merits some discussion in relation to the evolution of c/a which is different. If tetragonal ice VIII were to transform to a cubic structure by a second-order transition at low temperature the separation $\varepsilon=2c\,[\frac{1}{8}-z(\mathrm{O})]$ between the two hydrogen-bonded oxygen sublattices should go to zero, that is z(O) should increase to 0.125. As previously[14] discussed such is not the case in the pressure range up to 10 GPa. The calculations (Table III) show this increase to be expected only above 20 GPa or so, which is the pressure range where the decrease of the dipole interaction under pressure starts playing a role[2] in the stability of ice VIII and its transition to ice VII, and where the slope dp/dT starts assuming a nonzero negative slope. In any case, the apparent discrepancy between the behavior of c/a and z(O) with density cannot be solved without more experimental data in a higher-pressure range, preferably at low temperature.

B. Proton transfer potential

The last check on our calculation concerns its application to the variation under pressure of the frequency of the A_{1g} symmetric vibron of the O-H (O-D) pair of atoms.

In the periodic Hartree-Fock scheme only perfect crystals can be handled and therefore the calculated proton transfer potential corresponds to a collective antiferroelectric symmetric O-H stretching. In order to understand the relationship between this potential and the actual one and therefore to estimate the uncertainties introduced by the collective approach we will briefly recall the approach of Koehler and Gillis.[49] These authors model the crystal by a system of interacting anharmonic oscillators. Denoting by u_i the vibrational coordinate of the mode which is responsible for the phase order-disorder transition, the Hamiltonian can be expressed as

$$H=\sum_i -\frac{1}{2M}\frac{d^2}{du_i^2}+\frac{1}{2}au_i^2+4\phi u_i^4-\frac{1}{2}\sum_{ij}\chi_{ij}u_iu_j\ , \tag{10}$$

in which M is the reduced mass, a and ϕ the quadratic and quartic constants of the potential, and χ_{ij} the interaction constant coupling the displacements in the ith and jth cells. The problem is solved variationally by means of a Hartree ansatz which yields the one-particle effective Hamiltonian:

$$H(u)=-\frac{1}{2M}\frac{d^2}{du^2}+\frac{1}{2}au^2+4\phi u^4-\chi u\langle u\rangle\ . \tag{11}$$

χ is there the $k=0$ Fourier component of χ_{ij}. In ordered materials the quadratic constant, a, is negative, whereas the quartic one, ϕ, is positive. The average single-particle coordinate $\langle u\rangle$ depends upon the temperature: below the transition $\langle u\rangle\neq0$, and above $\langle u\rangle=0$. Therefore, in the ordered phase the potential is asymmetric due to a nonzero linear term while the disordered one is characterized by a symmetric double-well potential. In ice VII and ice VIII, the A_{1g} frequencies are very close and therefore the coupling coefficients are small. Therefore the error introduced by the collective approximation is expected to be at least one order of magnitude less than those due to the approximate nature of the Hartree-Fock approach.

These considerations allow the proton motion in the ordered phase to be represented by a collective antiferroelectric mode which is used to calculate the vibrational levels at Γ by the frozen phonon approach.[50] The proton transfer Born-Oppenheimer energy curve for the A_{1g} antiferroelectric collective mode has been calculated for several O-O distances corresponding to the pressures reported in Table III. Figure 9 presents the Born-Oppenheimer energy surface for the proton transfer as a function of pressure. The main feature of this graph is the lowering of the barrier at high pressure. However, there is no evidence for a single minimum potential in the pressure range investigated here. The energy levels have been calculated by a Lanczos-based collocation technique.[51] The potential energy curves have been fitted to fourth- and sixth-order polynomials for each O-O distance considered. The A_{1g} frequency shifts vs pressure are plotted in Fig. 10 for D_2O. The values for the frequencies of the A_{1g} vibron in D_2O ice VIII at ~260 K were obtained by Raman scattering in a diamond anvil

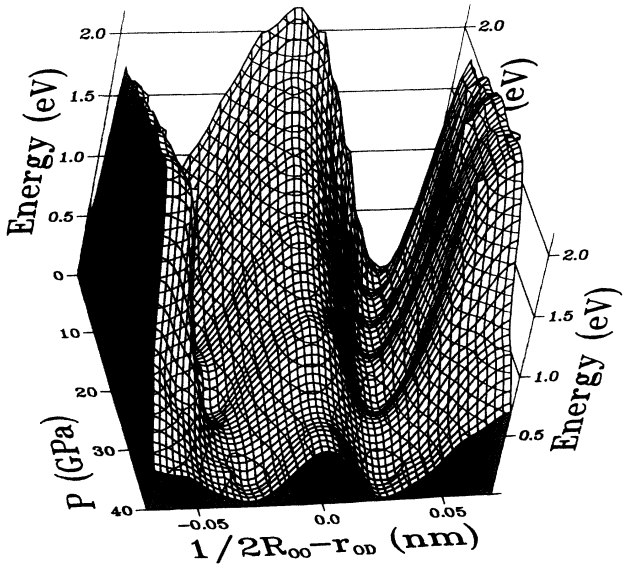

FIG. 9. Born-Oppenheimer energy surface for the deuteron transfer along the O-D-O direction *versus* pressure. Up to 30 GPa the decrease of the potential barrier at midpoint of the oxygens and the flattening out of the deuteron potential well is not accompanied by a noticeable increase of the O-D distance.

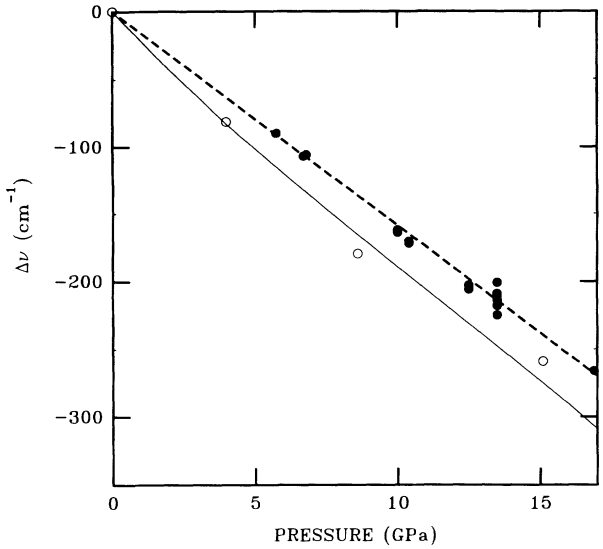

FIG. 10. Variation of the wave number of the A_{1g} vibron in D_2O VIII under pressure. Full circles and dashed line: Experiment. Extrapolation to ambient pressure ($\Delta\nu=0$) gives a wave number of $\nu=2650$ cm^{-1}. Empty circles: Calculation with anharmonic terms to sixth order.

cell in the course of the study reported in Ref. 2. The decrease in frequency is -16 cm^{-1} GPa^{-1}: that is almost identical to the value of -17 cm^{-1} GPa^{-1} found[52] in D_2O VII at room temperature. The decrease which we calculate here, using anharmonic terms to the sixth order is -18 cm^{-1}GPa^{-1}, which is in good agreement with experiment. The experimental results, as well as this calculation, contradict the belief widely spread in chemical physics that ν_{AH} frequency shifts are strongly correlated to lengthening of the A-H bond. It is therefore not necessary, as had been frequently proposed before, to assign the decrease of the stretching frequencies in H bonded solids to an increase of the covalent hydrogen bond length. This relation exists at ambient pressure and is well documented on a number of compounds[53] but the effect of high pressure in the present case is quite different.

VII. CONCLUSION

The behavior of the hydrogen bond length under pressure is useful information towards a prediction of the pressure of symmetrization of ices. The model used here, satisfactory as it may be in the range of pressure we examined, cannot be used at higher pressures where H_2O (or D_2O) will presumably lose its molecular character. The experimental evidence presented here does not permit a simple extrapolation to higher pressures. Nevertheless, the present evidence that the O-H bond length increases under pressure much more slowly than previously envisaged can only lead to the conclusion that the pressure for symmetrization should be higher than previously expected (50–80 GPa). This is entirely consistent with Raman-scattering measurements[2] which show that symmetrization does not occur below 72 GPa in D_2O VIII, in contrast with experimental[3,4] or theoretical[5–8] arguments, and yield an estimate of at least 100 GPa for the pressure where the hydrogen bond should disappear.

Precise knowledge of the effective potential of the proton in high-density matter is important not only for water ices but also for other simple molecules such as CH_4, NH_3 or H_2 itself, which make up over 80% of the mass of the planets in the solar system. In the earth itself, it has been estimated[54,55] that the mantle could contain the equivalent of one to four times the mass of water of all the oceans, in the form of H_2O, or OH^-. Thus the understanding of the hydrogen bond in very dense matter is important for planetary modeling, especially for the inner physicochemistry. Neutron-scattering methods, in the past few years have been shown to be applicable[21,56] above 20 GPa, and there is no doubt that structural studies will be feasible, in the near future, in a higher range of pressures, together with the use of variable temperature. This type of development, the continuing increase in the flux of neutron sources and the availability of better detection methods should bring to the study of very dense media the full power of elastic and inelastic neutron diffraction, in the same way as this field has benefited, in the past decades, from investigations by optical and x-ray methods.

Note added in proof. After this article was submitted, a similar method of calculation (Sec. V and Sec. VI B) by Ojamaë *et al.*[57] has been published which is in quantitative agreement with the calculations presented here.

ACKNOWLEDGMENTS

We would like to acknowledge the assistance of Dr. D. R. Allan, P. Grima, M. Gauthier, and Mr. J. Chauhan in carrying out the experiments and are grateful to Professor J. L. Finney for helpful discussions. We wish to thank Dr. M. Caffarel and Dr. P. Rudel for kindly providing the multidimensional Lanczos algorithm software. The support of the United Kingdom Science and Engineering Research Council, the French Commissariat à l'Energie Atomique under Contract No. WOO319/3255, and the Commission of the European Community under Twinning Contract No. SC1-CT91-0692 are also gratefully acknowledged. Physique des Milieux Condensés is Unité de Recherche Associée au CNRS No. 782. Laboratoire de Dynamique des Interactions Moléculaires is Unité Propre de Recherche au CNRS No. 271. The cell's prototype and bank of 90° detectors have been funded by the European Community under Science Contract No. SC1-CT91-0692. We thank Professor D. K. Ross, Dr. J. Li, and Dr. E. C. Bokhenkov for giving us access to their diffraction spectra on ice VIII at low temperature and allowing us to use them for our calculation.

[1]Ph. Pruzan, J. C. Chervin, and B. Canny, J. Chem. Phys. **97**, 718 (1992).

[2]Ph. Pruzan, J. C. Chervin, and B. Canny, J. Chem. Phys. **99**, 9842 (1993).

[3]K. R. Hirsch and W. B. Holzapfel, J. Chem. Phys. **84**, 2771 (1986).

[4]A. Polian and M. Grimsditch, Phys. Rev. Lett. **52**, 1312 (1984).

[5]W. B. Holzapfel, J. Chem. Phys. **56**, 712 (1971).

[6]F. H. Stillinger and K. S. Schweizer, J. Phys. Chem. **87**, 4281 (1983).
[7]K. S. Schweizer and F. H. Stillinger, J. Chem. Phys. **80**, 1230 (1984).
[8]C. Lee, D. Vanderbilt, K. Laasonen, R. Car, and M. Parrinello, Phys. Rev. B **47**, 4863 (1993).
[9]G. C. Pimentel and A. L. McClellan, *The Hydrogen Bond* (Freeman, San Francisco, 1960), p. 259.
[10]I. Olovson and P. G. Jönsson, in *The Hydrogen Bond—Recent Developments in Theory and Experiments,* edited by P. Schuster, G. Zundel, and C. Sandorfy (North-Holland, Amsterdam, 1976), Vol. II, p. 395.
[11]E. Matsushita and T. Matsubara, Prog. Theor. Phys. **67**, 1 (1982).
[12]G. E. Walrafen, M. Abebe, F. A. Mauer, S. Block, G. J. Piemarini, and R. Munroe, J. Chem. Phys. **77**, 2166 (1982).
[13]D. D. Klug and E. Whalley, J. Chem. Phys. **81**, 1220 (1984).
[14]R. J. Nelmes, J. S. Loveday, R. M. Wilson, J. M. Besson, Ph. Pruzan, S. Klotz, G. Hamel, and S. Hull, Phys. Rev. Lett. **71**, 1192 (1993).
[15]W. F. Kuhs, J. L. Finney, C. Vettier, and D. V. Bliss, J. Chem. Phys. **81**, 3612 (1984).
[16]J. D. Jorgensen, R. A. Beyerlein, N. Watanabe, and T. G. Worlton, J. Chem. Phys. **81**, 3211 (1984).
[17]L. G. Khvostantsev, High Temp. High Pressures **16**, 165 (1984).
[18]J. M. Besson, R. J. Nelmes, G. Hamel, J. S. Loveday, G. Weill, and S. Hull, Physica B **180&181**, 907 (1992).
[19]R. J. Nelmes, J. S. Loveday, and J. M. Besson, in *Accuracy in Powder Diffraction II,* Proceedings of the International Conference, edited by E. Prince and J. K. Staliek, National Institute of Standards and Technology Special Publication No. 846 (U.S. GPO, Washington, DC, 1992), p. 195.
[20]J. M. Besson, G. Weill, G. Hamel, R. J. Nelmes, J. S. Loveday, and S. Hull, Phys. Rev. B **45**, 2613 (1992).
[21]J. M. Besson, R. J. Nelmes, J. S. Loveday, G. Hamel, P. Pruzan, and S. Hull, High Pressure Res. **9**, 179 (1992).
[22]J. S. Loveday, R. Wilson, R. J. Nelmes, J. M. Besson, S. Klotz, G. Hamel, and S. Hull, in *High Pressure Science and Technology,* Proceedings of the 1993 Joint AIRAPT/APS Conference, Colorado Springs, Colorado, 1993, edited by S. C. Schmidt, J. W. Shaner, G. A. Samara, and M. Ross (American Institute of Physics, Woodbury, in press).
[23]S. Klotz, J. M. Besson, G. Hamel, R. J. Nelmes, J. S. Loveday, R. M. Wilson, and S. Hull, in *High Pressure Science and Technology* (Ref. 22).
[24]K. Yamamoto, Jpn. J. Appl. Phys. **21**, 567 (1982).
[25]R. B. von Dreele and A. C. Larson (unpublished).
[26]P. Vinet, J. Ferrante, J. R. Smith, and J. H. Rose, J. Phys. C **19**, L467 (1986).
[27]P. Vinet, J. R. Smith, J. Ferrante, and J. H. Rose, Phys. Rev. B **35**, 1945 (1987).
[28]R. J. Hemley, A. P. Jephcoat, H. K. Mao, C. S. Zha, L. W. Finger, and D. E. Cox, Nature (London) **330**, 737 (1987).
[29]R. G. Munro, S. Block, F. A. Mauer, and G. Piermarini, J. Appl. Phys. **53**, 6174 (1982).
[30]L. G. Liu, Earth Planet Sci. Lett. **61**, 359 (1982).
[31]B. Kamb and S. Prakash, as quoted in Ref. 15 and in *Ice Physics,* edited by P. V. Hobbs (Clarendon, Oxford, 1974).
[32]M. Jakob and S. Erk, *Properties of Ordinary Water Substance,* edited by N. E. Dorsey (Hafner, New York, 1968), p. 476.
[33]P. W. Bridgman, Proc. Am. Acad. Arts Sci. **48**, 307 (1912).
[34]R. S. Krishnan, R. Srinivasan, and S. Nevanaraganan, *Thermal Expansion of Crystals* (Pergamon, New York, 1979).
[35]R. Dovesi, V. R. Saunders, and C. Roetti (unpublished).
[36]C. Pisani, R. Dovesi, and C. Roetti, *Hartree-Fock ab initio Treatment of Crystalline Systems,* edited by G. Berthier *et al.*, Lecture Notes in Chemistry, Vol. 48 (Springer-Verlag, Berlin, 1988).
[37]W. J. Hehre, R. Ditchfield, and J. A. Pople, J. Chem. Phys. **56**, 2257 (1972).
[38]M. J. Frisch, J. E. Del Bene, J. S. Binkley, and H. F. Schafer III, J. Chem. Phys. **84**, 2279 (1986).
[39]G. Stollhoff and P. Fulde, J. Chem. Phys. **73**, 4548 (1980).
[40]R. G. Gordon and Y. S. Kim, J. Chem. Phys. **56**, 3122 (1972); Y. S. Kim and R. G. Gordon, **60**, 1842 (1974).
[41]R. Le Sar and R. G. Gordon, Phys. Rev. B **25**, 7221 (1982).
[42]M. S. Spackman, J. Chem. Phys. **85**, 6579 (1986).
[43]Ph. d'Arco, M. Causá, C. Roetti, and B. Silvi, Phys. Rev. B **47**, 3522 (1993).
[44]Ph. D'Arco (private communication).
[45]A. T. Amos and J. A. Yoffe, Chem. Phys. Lett. **39**, 53 (1976).
[46]D. J. Margoliash and W. J. Meath, J. Chem. Phys. **68**, 1426 (1978).
[47]S. F. Boys and F. Bernardi, Mol. Phys. **19**, 553 (1970).
[48]M. D. Morse and S. A. Rice, J. Chem. Phys. **76**, 650 (1982).
[49]T. R. Koehler and N. S. Gillis, Phys. Rev. B **7**, 4980 (1973).
[50]V. Heine and D. Weaire, in *Solid State Physics: Advances in Research and Applications,* edited by H. Ehrenreich, F. Seitz, and D. Turnbull (Academic, New York, 1970), Vol. 24, p. 249.
[51]C. Lanczos, J. Res. Nat. Bur. Stand. **45**, 255 (1970).
[52]Ph. Pruzan, J. C. Chervin, and M. Gauthier, Europhys. Lett. **13**, 81 (1990).
[53]A. Novak, in *Structure and Bonding,* edited by J. H. Fuhrhop, G. Blauer, T. J. R. Weakly, and A. Novak (Springer, Berlin, 1974), p. 197.
[54]T. J. Ahrens, Nature (London) **342**, 122 (1989).
[55]A. Jambon and J. L. Zimmermann, Earth Planet. Sci. Lett. **101**, 323 (1990).
[56]R. J. Nelmes and J. M. Besson (unpublished).
[57]L. Ojamaë, K. Hermansson, R. Dovesi, C. Roetti, and V. R. Saunders, J. Chem. Phys. **100**, 2128 (1994).

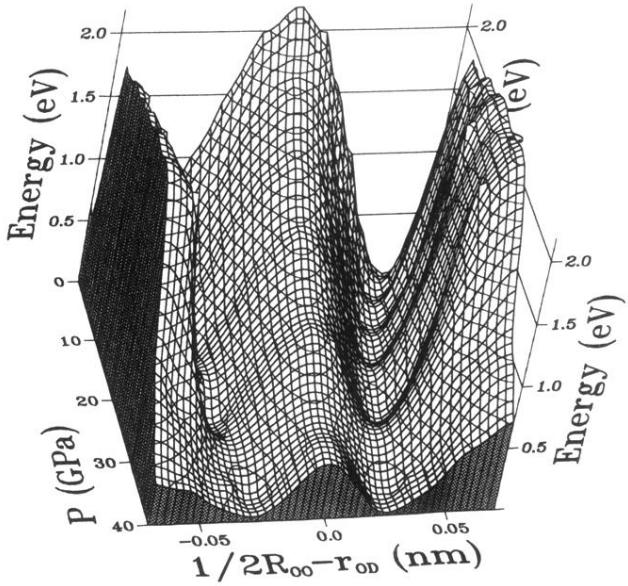

FIG. 9. Born-Oppenheimer energy surface for the deuteron transfer along the O-D-O direction *versus* pressure. Up to 30 GPa the decrease of the potential barrier at midpoint of the oxygens and the flattening out of the deuteron potential well is not accompanied by a noticeable increase of the O-D distance.